First-principles studies on the pressure dependences of the stress–strain relationship and elastic stability of semiconductors

2006 J. Phys.: Condens. Matter 18 395

(http://iopscience.iop.org/0953-8984/18/2/004)

INSTITUTE OF PHYSICS PUBLISHING JOURNAL OF PHYSICS: CONDENSED MATTER

J. Phys.: Condens. Matter **18** (2006) 395–409 doi:10.1088/0953-8984/18/2/004

First-principles studies on the pressure dependences of the stress–strain relationship and elastic stability of semiconductors

S Q Wang[1,2], H Q Ye[1] and S Yip[2]

[1] Shenyang National Laboratory for Materials Science, Institute of Metal Research, Chinese Academy of Sciences, 72 Wenhua Road, Shenyang 110016, People's Republic of China
[2] Department of Nuclear Engineering, Massachusetts Institute of Technology, Cambridge, MA 02139, USA

E-mail: sqwang@imr.ac.cn

Received 31 July 2005, in final form 1 August 2005
Published 14 December 2005
Online at stacks.iop.org/JPhysCM/18/395

Abstract

We investigate the stress–strain relationship and elastic stability of zinc-blende GaP, GaN, InP and BN lattices under hydrostatic pressure by first-principles calculation. A simple and direct *ab initio* implementation for studying the mechanical properties of cubic crystals is developed. The four phases' full-set stress–strain coefficients in wide pressure ranges are theoretically calculated. The fundamental mechanism of elastic stability and the origin of phase transformation under hydrostatic pressure are explored. We found that the abilities for most of these lattices are enhanced to sustain axial strain but weaken to shear strain under higher pressure. The conditions of lattice stability are analysed using both the thermodynamic work–energy criterion and the elastic-stiffness criteria. We show that the lattice collapse of the perfect crystals is caused by the disappearance of their bulk moduli under volume dilation. Lattice defects are considered to be the main reason causing phase transformation under pressure. The correlation between the phonon softening and the variation of elastic coefficients is studied. The pressure dependence of the Kleinman internal strain parameter and its relationship to elastic stability is also explored.

1. Introduction

Mechanical or elastic stability is an important issue for understanding the elastic behaviour and phase transformation of solids [1–4]. In 1940 Born presented the first systematic investigation of lattice stability and put forward a stability criterion by requiring convexity for an expansion of the internal energy of a crystal in a power series in the strain [1]. Later, Hill *et al* showed that the stability is relevant to the actual realization for applying strain [2, 5]. From a path-dependent Gibbs integral analysis Wang *et al* [3, 6] suggested the stiffness-coefficient criteria.

Morris *et al* [4] considered the Helmholtz free energy change under strain and obtained similar criteria as Wang *et al*. Theoretical studies of lattice stabilities have been carried out for Si [7–9], SiC [7, 8, 10, 11], Au [3, 6] and Ni_3Al [12] by classical molecular dynamics simulation. Stability criteria have also been extensively used in theoretical estimates of the ideal strength of various materials [13–20] through first-principles calculation. However, the microscopic mechanism of lattice stability continues to be an outstanding issue.

We have recently reported some theoretical investigations of the mechanical, dielectric and elastic properties of groups III–V and IV semiconductors by first-principles calculations [21–25]. In this work we studied the problem of the stress–strain relationship and elastic stability of four typical III–V semiconductors in zinc-blende (ZB) structure under hydrostatic pressure by first-principles plane-wave pseudopotential calculation. Most of the semiconductors have their stable geometrical configuration as ZB symmetry in ambient environment. Phase transformation from ZB to more ionic octet phases, such as the NaCl structure and the CsCl structure, usually occurs for semiconductors when their original structures lose stability under pressure [26–28]. The aim of the present study is to explore the influence of hydrostatic pressure on elastic instability and the origin of the phase transformation in ZB crystals.

The paper is organized as follows. In section 2, the details of first-principles calculations of strain, stress and elastic parameters are described. Our theoretical results and analyses on the relationship between elastic stability and pressure are given in section 3. In section 4, we discuss the connection between elastic stability and phase transformation. Finally, the summary and conclusions of the present work are given in section 5.

2. Details of first-principles calculation

Our study is based on the plane-wave pseudopotential method using the ABINIT computer code [29] with the Hartwigsen–Goedecker–Hutter (HGH) relativistic separable dual-space Gaussian pseudopotentials [30] in the local-density approximation. The effect of hydrostatic pressure is simulated by a symmetrical volume reduction of the lattice cell $V = (a/a_0)^3 V_0$ [21, 31]. a and a_0 respectively are the equilibrium lattice constants at pressure P and $P = 0$. Some key points of the present technical implementation are given below.

2.1. Strain modes

Strain is applied by exerting a small deformation of the lattice. The strain vector $\mathbf{e}$ relates to the strain tensor ε by

$$\varepsilon = \begin{pmatrix} e_1 & e_6/2 & e_5/2 \\ e_6/2 & e_2 & e_4/2 \\ e_5/2 & e_4/2 & e_3 \end{pmatrix}. \tag{1}$$

The strain causes a change in the primitive vectors of the lattice cell by

$$\begin{pmatrix} \mathbf{a}_1' \\ \mathbf{a}_2' \\ \mathbf{a}_3' \end{pmatrix} = \begin{pmatrix} \mathbf{a}_1 \\ \mathbf{a}_2 \\ \mathbf{a}_3 \end{pmatrix} \cdot (\mathbf{I} + \varepsilon). \tag{2}$$

The following four modes [23, 24] of applying strain on the lattice are used in the present study.

Mode 1: Bi-axial strain at [100] and [010] directions $\mathbf{e} = (\delta, \delta, 0, 0, 0, 0)$,
Mode 2: Pure [111] shear strain $\mathbf{e} = (0, 0, 0, \delta, \delta, \delta)$.
Mode 3: Volume-conserving tetragonal strain $\mathbf{e} = (\delta, -\delta, \delta^2/(1-\delta^2), 0, 0, 0)$,
Mode 4: Isotropic volume dilatation $\mathbf{e} = (\delta, \delta, \delta, 0, 0, 0)$,

2.2. Stress calculation

The technique of *ab initio* calculation of stress had been developed by Nielsen and Martin [32, 33]. The stress tensor σ_{ij} $(i, j = 1 \ldots 3)$ is defined as the derivative of the total energy with respect to the strain tensor ε_{ij} $(i, j = 1 \ldots 3)$ of the system,

$$\sigma_{ij} = \Omega^{-1} \frac{\partial E_{\text{tot}}}{\partial \varepsilon_{ij}}, \tag{3}$$

where Ω is the volume of the unit cell. The total energy E_{tot} per unit cell in the local-density approximation is calculated by

$$\begin{aligned} E_{\text{tot}} = {} & \sum_{\mathbf{k},\mathbf{G},i} |\Psi_i(\mathbf{k}+\mathbf{G})|^2 \frac{\hbar^2}{2m}(\mathbf{k}+\mathbf{G})^2 + \frac{1}{2}4\pi e^2 \sum\nolimits'_{\mathbf{G}} \frac{|\rho(\mathbf{G})|}{G^2} \\ & + \sum_{\mathbf{G}} \varepsilon_{xc}(\mathbf{G})\rho^*(\mathbf{G}) + \sum_{\mathbf{G},\tau} S_\tau(\mathbf{G}) V_\tau^{\text{L}}(\mathbf{G})\rho^*(\mathbf{G}) \\ & + \sum_{\mathbf{k},\mathbf{G},\mathbf{G}',i,l,\tau} S_\tau(\mathbf{G}-\mathbf{G}')\Delta V_{l,\tau}^{\text{NL}}(\mathbf{k}+\mathbf{G},\mathbf{k}+\mathbf{G}')\Psi_i(\mathbf{k}+\mathbf{G})\Psi_i^*(\mathbf{k}+\mathbf{G}) \\ & + \left(\sum_\tau \alpha_\tau\right)\left(\Omega^{-1}\sum_\tau Z_\tau\right) + \Omega^{-1}\gamma_{\text{Ewarld}}. \end{aligned} \tag{4}$$

where Ψ is the wavefunction, $\mathbf{k}$ and $\mathbf{G}$ the reciprocal-lattice vectors, ρ the charge density, and S_τ $(\mathbf{G})$ is the structure factor. V^{L} and ΔV^{NL} are respectively the local and nonlocal corrections of the potential. Z_r is the ionic charge; γ_{Ewald} is the Madelung energy of ions of the crystal. The isotropic pressure is given by $P = -\sigma_{ii}$ $(i = 1, 2, 3)$ for the hydrostatic environment.

2.3. Stress–strain coefficients under pressure

Let ε_{ij} be the symmetric Lagrangian strain between the two configurations from $\mathbf{X}$ to $\mathbf{x}$, then the stress–strain relation is defined by

$$\sigma_{ij}(\mathbf{x}) = \sigma_{ij}(\mathbf{X}) + \sum_{kl} B_{ijkl}\varepsilon_{kl} + \cdots \tag{5}$$

where B_{ijkl} $(i, j, k, l = 1 \ldots 3)$ are the stress–strain coefficients or elastic-stiffness coefficients [34]. The terms $+\cdots$ are for the higher order of the strains. Due to the symmetric property in their two pairs of Cartesian indices, they can be expressed in Voigt notation as a 6×6 matrix $B_{\alpha\beta}$ $(\alpha, \beta = 1 \ldots 6)$. This matrix is not symmetric in general, i.e. $B_{\alpha\beta} \neq B_{\beta\alpha}$. However, the matrix is simplified to a symmetric form for the cubic crystal. The number of non-zero elements of stress–strain coefficients is reduced to three, namely B_{11}, B_{12} and B_{44}, in the cubic system. Besides, two more elastic-stiffness coefficients, B' and B_{b}, are defined in the present study. B_{b} is the bulk modulus at P. B' measures the lattice's resistance to in-plane shear. The relationships of these two coefficients to B_{11} and B_{12} are given by

$$\begin{aligned} B_{\text{b}} &= \frac{B_{11} + 2B_{12}}{3} \\ B' &= \frac{B_{11} - B_{12}}{2}. \end{aligned} \tag{6}$$

According to equation (5), the stress–strain coefficients B_{11} and B_{12} for a cubic crystal under hydrostatic pressure are calculated by applying a small *mode 1* strain, which gives

$$\begin{aligned} B_{11} &= \frac{\sigma_{11}(\mathbf{x}) - P(\mathbf{X})}{\delta} - B_{12}, \\ B_{12} &= \frac{\sigma_{33}(\mathbf{x}) - P(\mathbf{X})}{2\delta} \end{aligned} \tag{7}$$

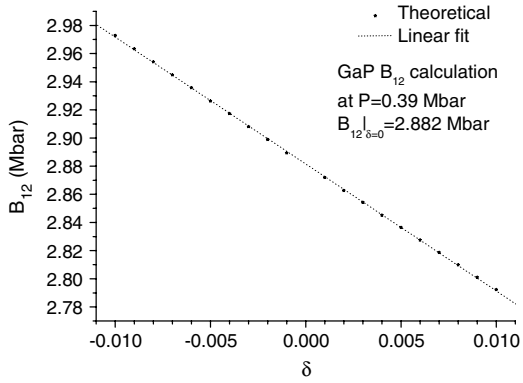

Figure 1. Illustration of the calculation of elastic stiffness coefficient B_{12} for the GaP phase. The elastic stiffness coefficient is a linear function of strain parameter δ. B_{12} is obtained by linear fitting of the first-principles B_{12} (δ) data and taking the value at $\delta = 0$ of the fitted equation.

where $P(\mathbf{X})$ is the hydrostatic pressure at $\mathbf{X}$, $P(\mathbf{X}) = \sigma_{ii}$ $(\mathbf{X})$ $(ii = 11, 22, 33)$. The pressure causes a cell volume change from V_0 to V. These pressure data are taken as the environmental hydrostatic pressure and keep constant throughout the subsequent strain calculation from $\mathbf{X}$ to $\mathbf{x}$. B_{44} is calculated by applying the *mode 2* strain

$$B_{44} = \frac{\sigma_{ij}(\mathbf{x})}{\delta}, \tag{8}$$

where $\sigma_{ij}(\mathbf{x})$ $(i \neq j)$ are the off-diagonal elements. All of these elements have the same value under this strain mode. B' can be calculated by applying *mode 3* strain

$$B' = \frac{(1+\delta)^2(\sigma_{11}(\mathbf{x}) - \sigma_{33}(\mathbf{x}))}{2\delta(3+3\delta+\delta^2)}. \tag{9}$$

The *mode 4* strain is used to calculate the bulk stiffness coefficient B_b:

$$B_\mathrm{b} = \frac{\sigma_{ii}(\mathbf{x})}{\delta}. \tag{10}$$

The theoretical elastic-stiffness coefficients vary slightly with strain parameter δ in the calculation. To eliminate this problem, we calculate 20 sets of data by varying δ from -0.01 to 0.01 at intervals of 0.001 (without $\delta = 0.00$). A linear relationship exists in these data. Our final stiffness coefficients are obtained by a linear fitting of the 20 sets of first-principles data and taking the value at $\delta = 0$ from the fitted equation. The coefficients calculated in this way are exactly the elastic-stiffness coefficients at pressure P. Figure 1 shows an example for the calculation of the B_{12} coefficient of GaP at $P = 0.39$ Mbar.

3. Results and analysis

3.1. Analysis of the first-principles pressure–volume relation

The pressure–volume relationship is the basis of the equation of state (EOS) of a material. It is necessary to examine the reliability of the pressure and stress data from first-principles calculation by direct comparison with relevant experimental results at the beginning of the present study. The experimental data of bulk modulus B_0 and its pressure derivative B_0' at $P = 0$ for ZB GaP [35] are 0.911 Mbar and 4.5, respectively. Figure 2 shows our comparison

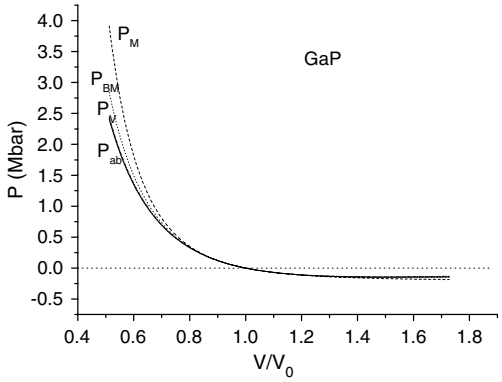

Figure 2. Comparison between the experimental and theoretical P–V/V_0 curves of GaP. The P_{ab} curve is from first-principles calculation based on the *ab initio* stress theory. P_{M}, P_{BM} and P_{V} are respectively calculated by Murnaghan, Birch–Murnaghan and the universal Vinet EOSs using the parameters from experiment.

between the experimental and theoretical P–V/V_0 curves, where P_{ab} is the curve from our first-principles stress calculation, P_{M}, P_{BM} and P_{V} are respectively calculated by the Murnaghan EOS [22]

$$P_M = \frac{B_0}{B_0'}\left[\left(\frac{V_0}{V}\right)^{B_0'} - 1\right], \tag{11}$$

the third-order Birch–Murnaghan equation [36]

$$P_{\mathrm{BM}} = \left(\frac{3}{2}\right) B_0 \left[\left(\frac{V_0}{V}\right)^{\frac{7}{3}} - \left(\frac{V_0}{V}\right)^{\frac{5}{3}}\right]\left\{1 - \left(\frac{3}{4}\right)(4 - B_0')\left[\left(\frac{V_0}{V}\right)^{\frac{2}{3}} - 1\right]\right\}, \tag{12}$$

and the universal EOS of Vinet *et al* [37]

$$P_{\mathrm{V}} = 3B_0 \frac{\left(1 - \left(\frac{V}{V_0}\right)^{\frac{1}{3}}\right)}{\left(\frac{V}{V_0}\right)^{\frac{2}{3}}} \mathrm{e}^{\left(\frac{3}{2}\right)(B_0'-1)\left(1-\left(\frac{V}{V_0}\right)^{\frac{1}{3}}\right)}, \tag{13}$$

using the experimental B_0 and B_0' data. The Birch-Murnaghan EOS is the high order approximation of the Murnaghan EOS. The Vinet EOS is considered to be able to accurately estimate the volume change of most solids under very high compression. It is seen that the P_{ab} curve is quite close to the empirical P_{V} and P_{BM} curves for large volume variation. Therefore, the reliability of our first-principles pressure and stress data is established.

3.2. Elastic stability under pressure

It is common knowledge that a perfect crystal becomes structurally unstable when the lattice can no longer withstand the applied external stress. Plastic deformation with the emergence of lattice defects or phase transformation will occur at this point. However, due to the existence of various lattice defects in real materials, the structure change may start well before this theoretical critical point. According to the theory of continuum mechanics, the thermodynamic stability condition for any mechanical system is given by the following equation [4–6]:

$$\Delta F \geqslant \Delta W. \tag{14}$$

This equation indicates that as a system is subject to a small transformation from state A to state B, it can maintain stability only when the increment of Helmholtz free energy ΔF of the system equals or exceeds the mechanical work ΔW done by the external force. For the present first-principles study at absolute zero temperature, the stability condition is simplified to

$$\Delta E_{\text{tot}} \geqslant \Delta W. \tag{15}$$

ΔE_{tot} is the change of total *ab initio* energy. The general form of ΔW is given by

$$\Delta W = \int_{\text{V}} \left(\varepsilon_{ij}\sigma_{ij} - \int_0^{\sigma_{ij}} \varepsilon_{ij} d\sigma_{ij} \right) \text{d}V. \tag{16}$$

For the system under isotropic hydrostatic pressure, the work ΔW done by constant isotropic pressure P for a small cell volume variation ΔV is simplified as

$$\Delta W = -P\Delta V. \tag{17}$$

The calculation of ΔW is independent of the way the volume changes for the constant hydrostatic pressure condition. Then, the elastic stability condition becomes

$$\Delta E_{\text{tot}} + P\Delta V \geqslant 0 \tag{18}$$

where the internal energy change ΔE_{tot}, caused by a small strain ε under the isotropic pressure P, is directly available from first-principles calculation. The cell-volume change ΔV is calculated by $\Delta V = \mathbf{a}_1' \cdot (\mathbf{a}_2' \times \mathbf{a}_3') - \mathbf{a}_1 \cdot (\mathbf{a}_2 \times \mathbf{a}_3)$. Therefore, the condition of elastic stability of equation (18) can be conveniently examined in the present first-principles calculation. This is the work–energy criterion for elastic stability analysis.

Figure 3 shows our results for the relationship between $\Delta E_{\text{tot}} + P\Delta V$ and strain parameter δ under three different strain modes for the GaP phase. It is seen that the critical points to keep equation (18) are at $P = 1.41$ Mbar for *mode 2*, $P = 1.41$ Mbar for *mode 3* and $a/a_0 = 1.148$ for *mode 4*, respectively. Equation (18) is no longer valid when P or a/a_0 is higher than these values and the lattice becomes structurally unstable. A similar result on elastic stability analysis for the InP phase is presented in figure 4. The critical points for this phase are at $P = 0.75$ Mbar for *mode 2*, $P = 0.67$ Mbar for *mode 3* and $a/a_0 = 1.146$ for *mode 4*, respectively.

3.3. Pressure dependence of elastic-stiffness coefficients

The investigation of elastic stability of solids has been frequently approached by elastic-stiffness coefficient calculation [3, 6, 7]. Wang *et al* [3, 6] proposed the following elastic-stiffness criteria for elastic stability of cubic crystals,

$$\begin{aligned} &B_{44} \geqslant 0 \\ &B_{11} - B_{12} \geqslant 0 \\ &B_{11} + 2B_{12} \geqslant 0, \end{aligned} \tag{19}$$

or

$$\begin{aligned} &B_{44} \geqslant 0 \\ &B' \geqslant 0 \\ &B_{\text{b}} \geqslant 0, \end{aligned} \tag{20}$$

by taking equation (6) into consideration. The *ab initio* elastic-stiffness coefficients can be conveniently calculated in the present study. It is worthwhile to compare the results of stability analysis from different approaches for a more complete understanding of the problem.

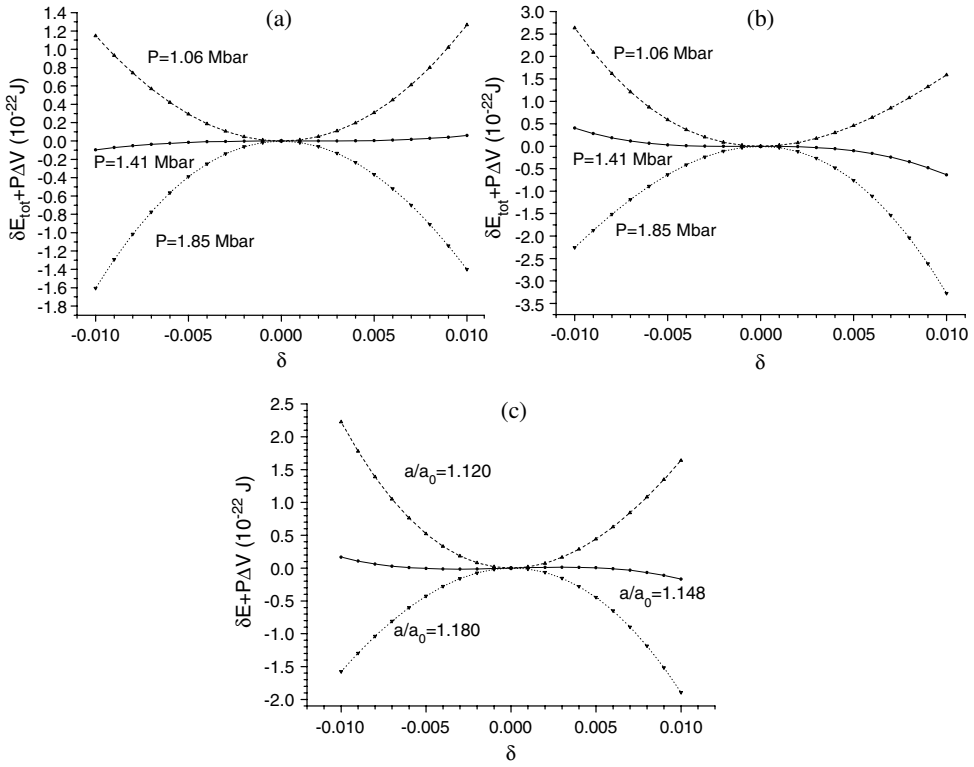

Figure 3. Theoretical relationship between $\Delta E_{\rm tot} + P\Delta V$ and strain parameter δ under strain *mode 2* (a), *mode 3* (b) and *mode 4* (c), respectively, for GaP phase.

The pressure dependences of elastic-stiffness coefficients of ZB GaP, InP, BN and GaN are calculated following the principles in section 2.3. Figures 5(a)–(d) show our first-principles results on the variations of elastic-stiffness coefficients with pressure for these phases. It is seen from the figure that B_{11}, B_{12} and $B_{\rm b}$ monotonically increase with pressure, while B_{44} and B' may increase or decrease for different phases. In GaP and InP, B_{44} decreases more rapidly than B'. These two coefficients always increase up to $P = 8.06$ Mbar for the BN phase. The points where B_{44} becomes zero are determined at $P = 1.41, 4.54$ and 0.75 Mbar for GaP, GaN and InP, respectively. Those points for B' are respectively at $P = 1.41, 2.19$ and 0.67 Mbar in the same phase order. B' always decreases to zero before B_{44} under pressure in these phases. B_{12} and $B_{\rm b}$ usually become higher under high pressure for GaP, GaN and InP. Meanwhile, B_{11} of BN has the largest value among all of its coefficients. This behaviour can be explained by the fact that bond bending is extraordinarily difficult in BN due to its quite small Kleinman internal strain parameter [24].

The stiffness coefficients vary with pressure P quite rapidly as cell volume increases. For a better description of this behaviour, the variations of elastic-stiffness coefficients with lattice dimension a/a_0 are presented in figures 6(a)–(d). It is seen that B_{12} becomes lowest in a wide range, indicating that these phases are weakest in resistance to in-plane shear under volume dilatation. The a/a_0 values at $B_{12} = 0$ are determined from figure 6 to be 1.081, 1.085, 1.088 and 1.062 for GaP, GaN, InP and BN, respectively. $B_{\rm b}$ becomes zero next to B_{12} at $a/a_0 = 1.148$, 1.147, 1.146 and 1.153 in the same order. According to the stability criteria of equation (20) the lattice becomes elastically unstable when the elastic-stiffness coefficients

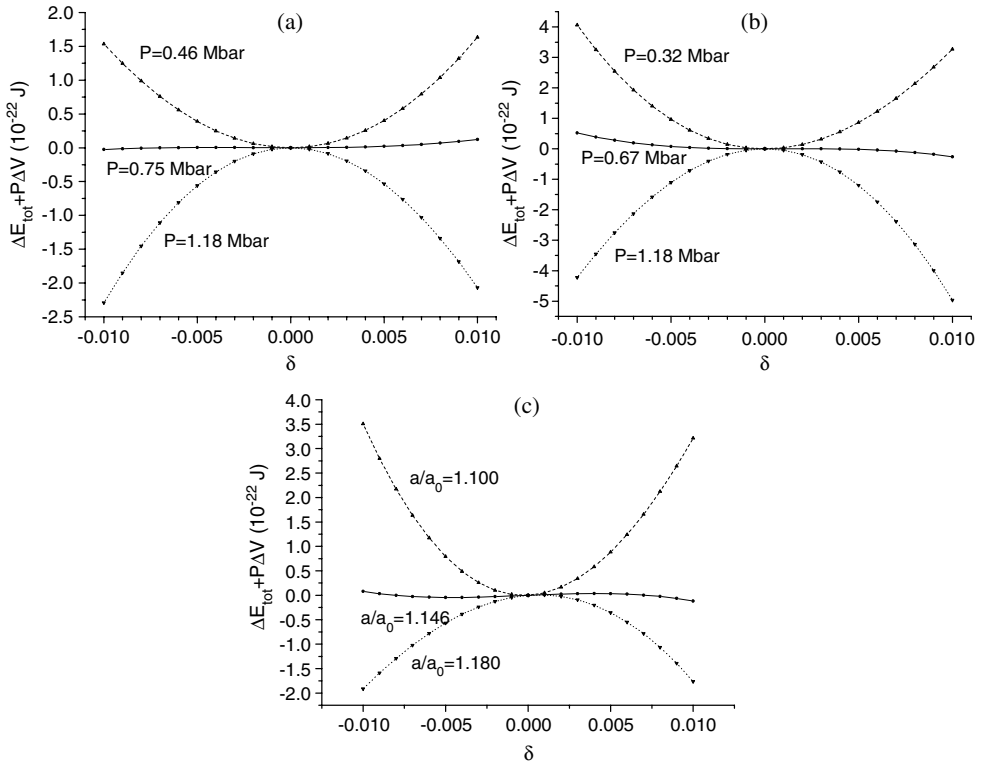

Figure 4. Theoretical relationship between $\Delta E_{\rm tot} + P\Delta V$ and strain parameter δ under strain *mode 2* (a), *mode 3* (b) and *mode 4* (c), respectively, for InP phase.

B_{44}, B' and $B_{\rm b}$ become zero. By comparing present results with those in section 3.2, it is seen that these two ways of analysing elastic stability give the same results for the conditions of structure stability for GaP and InP under hydrostatic pressure. Actually, since the elastic-stiffness criteria in equation (19) are specifically deduced from the work–energy criterion of equation (15) for cubic phases, they are strictly equivalent theoretically. Therefore, it should be a natural matter for the above consistent results of elastic stability analyses. Besides, the present work also demonstrates the efficiency and reliability of the two first-principles realizations in the study of pressure-dependent structure stability.

3.4. Pressure dependences of internal elasticity and Kleinman internal strain parameter

Internal elasticity exists for crystals lacking inversion symmetry under structure deformation. It is necessary to study the effect of internal elasticity on the elastic stability of crystals. Due to the restriction in crystallographic symmetry, the internal strain has only one degree of freedom for the phase with ZB structure. This variable measures the relative displacement between the two sub-lattices in the ZB phase and is commonly presented by the Kleinman internal strain parameter ζ [38]. Under [111] shear strain of *mode 2*, the elongation of the [111] bond is given by $(1-\zeta)\delta a\sqrt{3}/4$. Our implementation for *ab initio* calculation of Kleinman parameter ζ is available elsewhere [24]. The calculated *ab initio* ζ–a/a_0 relationships for the four phases are shown in figure 7. The pressure variation of ζ can be readily given through the EOS equation of respective phases from the figure. It is seen from the comparison of our calculated ζ data at $P = 0$ with previous publications in table 1 that the accordance is quite good. The ζ

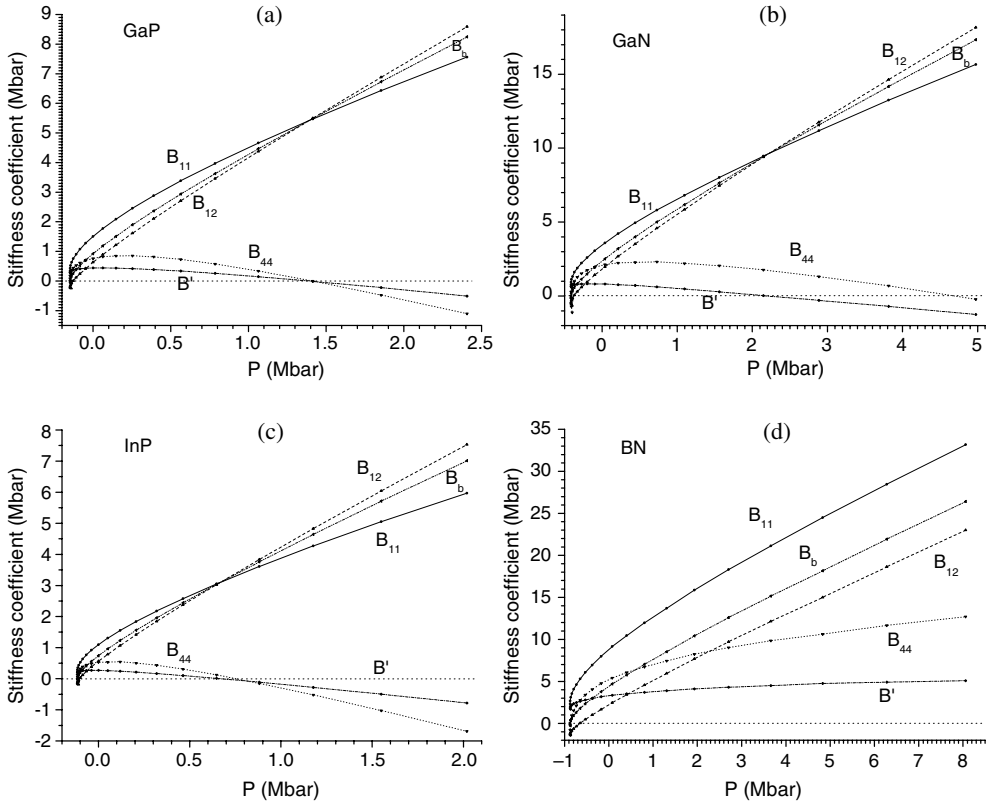

Figure 5. Relationship between elastic-stiffness coefficient and P for GaP (a), GaN (b), InP (c) and BN (d), respectively.

Table 1. Kleinman internal strain parameters at $P = 0.0$ Mbar for GaP, GaN, InP and BN in ZB structure.

	Present calc.	Other calc.
GaP	0.526	0.533 [40], 0.516 [24][a]
GaN	0.482	0.5 [39], 0.477 [24][a]
InP	0.615	0.652 [40], 0.59 [41], 0.615 [24][a]
BN	0.130	0.11 [42], 0.1 [39],0.117 [24][a]

[a] We used a coarse δ interval to calculate the ζ parameter in [24]. The present results are considered more accurate.

parameter is considered to fall in the range between 0 and 1 under ambient conditions, where $\zeta = 1$ corresponds to the rigid bond connection among atoms, and $\zeta = 0$ is for the case of a sublattice subject to an affine transformation with the macroscopic strain. However, it is seen by combination of figures 6 and 7 that the lattice can keep stable with ζ up to 1.149, 1.098, 1.127 and 1.066 respectively for GaP, GaN, InP and BN under high pressure. The present results also show that ζ may gain negative values of -0.416, -1.136, -0.438 and -1.439 respectively for GaP, GaN, InP and BN before structure failure under volume dilatation.

The relationship between total and internal elastic coefficients for ZB phase is given by [33, 43–46]

$$B_{44} = B_{44}^0 - A^2 E_{11} \tag{21}$$

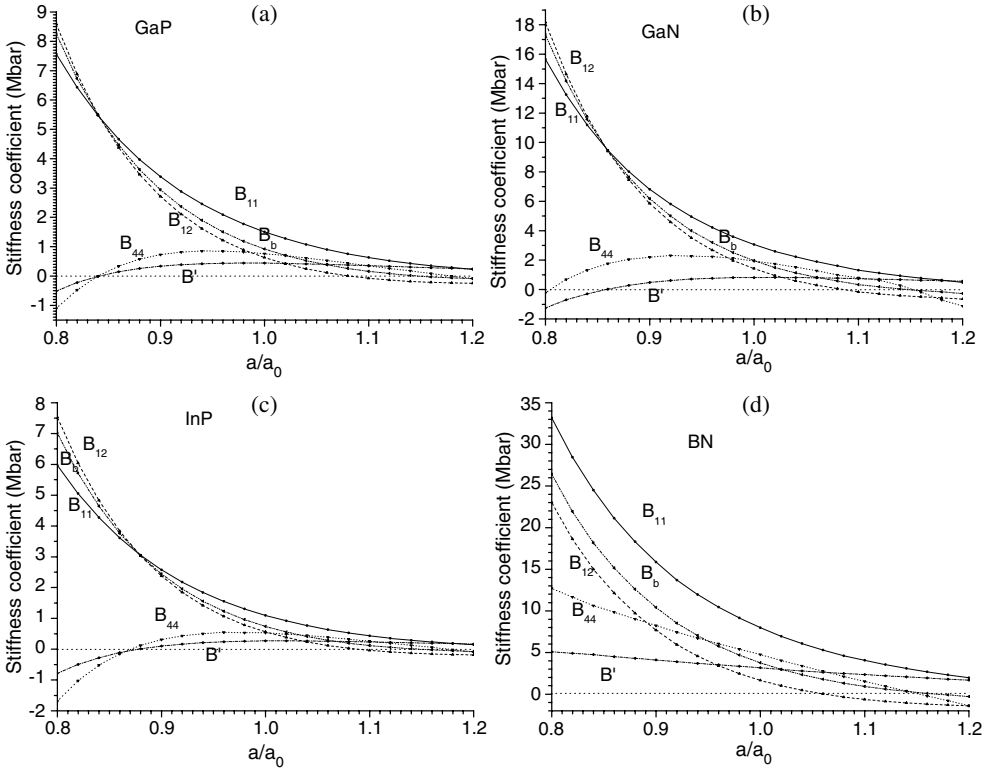

Figure 6. Relationship between elastic-stiffness coefficient and a/a_0 for GaP (a), GaN (b), InP (c) and BN (d), respectively.

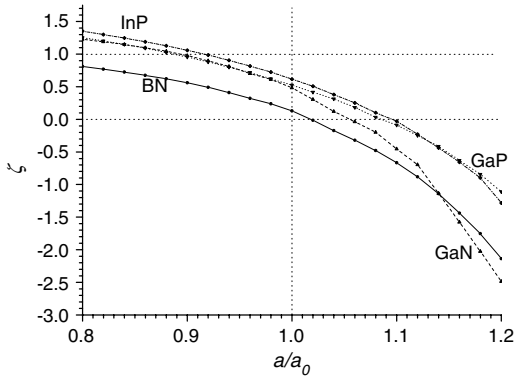

Figure 7. Relationship between Kleinman internal strain parameter and a/a_0 of GaP, GaN, InP and BN.

where B_{44}^0 is the elastic coefficient in the absence of internal displacement, $A = -a\zeta/4$. E_{11} is the only independent internal elastic coefficient of the ZB phase. We calculated the pressure dependence of B_{44}^0 by forbidding internal ion relaxation under *mode 2* strain. As an example, the B_{44}^0–a/a_0 curve of ZB InP is presented in figure 8. From the theoretical data of B_{44}, B_{44}^0 and ζ, the internal elastic coefficient E_{11} can be conveniently calculated by equation (21). Figure 9

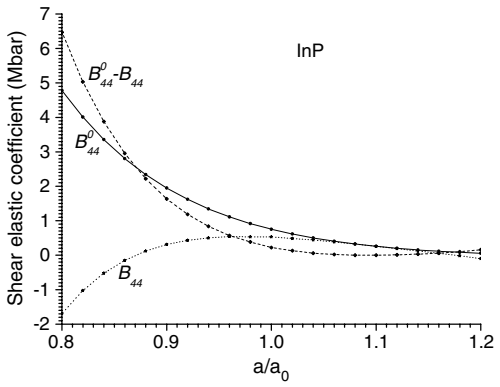

Figure 8. The *ab intio* B^0_{44}–a/a_0 curve of ZB InP.

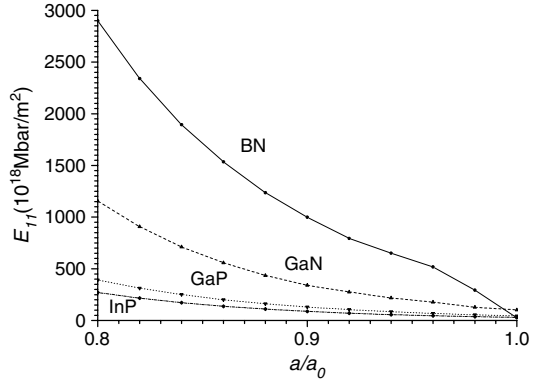

Figure 9. The *ab initio* E_{11}–a/a_0 relationships of GaP, GaN, InP and BN phases.

presents the *ab initio* E_{11}–a/a_0 relationships of GaP, GaN, InP and BN phases. It is seen from the figure that the internal elastic coefficient monotonically increases with pressure in general. The BN phase shows the smallest ζ and largest E_{11}, which indicates that the bond-bending is the main factor in internal elasticity.

4. Discussion

There are several critical points of elastic instability for the phases studied here. It is essential to know which one is the true failure point of the actual material. In the case of lattice dilatation, B_{12} is always the first one to decrease to zero in these four III–V phases. This indicates that these phases are quite weak against in-plane shear. However, the crystal does not necessarily break down when this kind of shear in not present. In the following study the work–energy criterion is used to explore when these phases become structurally unstable under pure volume dilatation. In our calculation, the lattice parameter a is varied from a_0 to $1.2a_0$ at an increment of $0.001a_0$. Since the pressure is no longer constant under pure volume dilatation, the external work done during the procedure is calculated by

$$\Delta W = -\int_{\mathrm{V}}^{V'} P(V)\,\mathrm{d}V \tag{22}$$

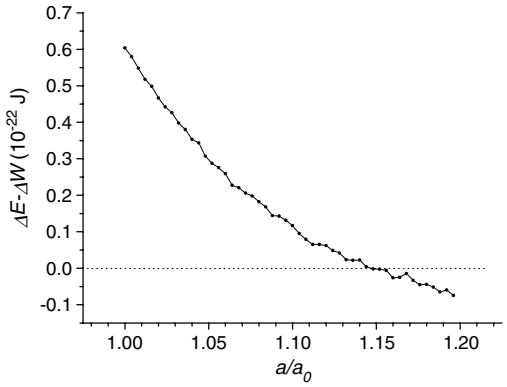

Figure 10. The first-principles curve of ΔE–ΔW versus a/a_0 for structural stability analysis of GaP phase.

where V and V' are the initial and the dilated cell volumes, respectively. We calculate the variation of internal energy increment ΔE and the external work ΔW after every four increments. The integral in equation (22) is approximately calculated by the numerical integral from these four sets of data. The theoretical curves of $\Delta E - \Delta W$ to a/a_0 for GaP are presented in figure 10. It is seen from the figure that equation (15) is violated when $a/a_0 > 1.148$. This critical point is just the same as the bulk modulus B_b becoming negative under lattice dilatation for ZB GaP. Therefore, the vanishing of the bulk modulus is the fundamental reason for lattice collapse under volume dilatation. The present conclusion is consistent with our previous results on the spinodal instability [3, 6].

To explore the details of elastic stability under positive hydrostatic pressure further, we investigate the pressure dependences of phonon bands of III–V phases in the ZB structure by first-principles response-function calculation [47]. Our calculated results for the ZB phases of GaN and BN are presented in figures 11(a) and (b), where the solid curves are the phonon bands at $P = 0$ Mbar, the dotted curves are the phonon bands at $P = 2.19$ Mbar ($a/a0 = 0.86$) and $P = 8.06$ Mbar ($a/a0 = 0.80$) for GaN and BN, respectively. It is seen from figure 11(a) that some parts of the lowest transverse acoustic branches of the GaN phonon become negative at $P = 2.19$ Mbar, indicating a softening of these phonons under pressure. We have shown in section 3.3 that the elastic coefficient B' of GaN becomes zero at this pressure. Therefore, the diminishing to zero of B' is considered as the main reason for phonon softening under pressure in GaN phases. It also shows that elastic instability exists together with the phenomenon of phonon softening in crystals. Since the elastic-stiffness coefficients always increase up to $P = 8.06$ Mbar for the ZB BN phase, there is no phonon softening observed at this pressure in figure 11(b). Recently, Prikhodko *et al* studied the pressure dependence of the elastic parameters and the sound velocities of 3C-SiC. They established a connection between phonon softening, sound velocity softening and phase transformation of the phase. Their results show that the most obvious phonon softening is along the Γ–K direction and the Gruneisen parameter of the lowest acoustic phonon at X is negative [48]. Our present results are in good agreement with theirs.

B_b always increases under positive hydrostatic pressure. However, the reduction of B_{44} and B' reflects that the stability of these phases is most sensitive to shear strain at high pressure. The reason can be properly understood as follows. The crystal lattice of the ZB phase is just like a highly compressed spring system under pressure. The stronger the isotropic force applied, the

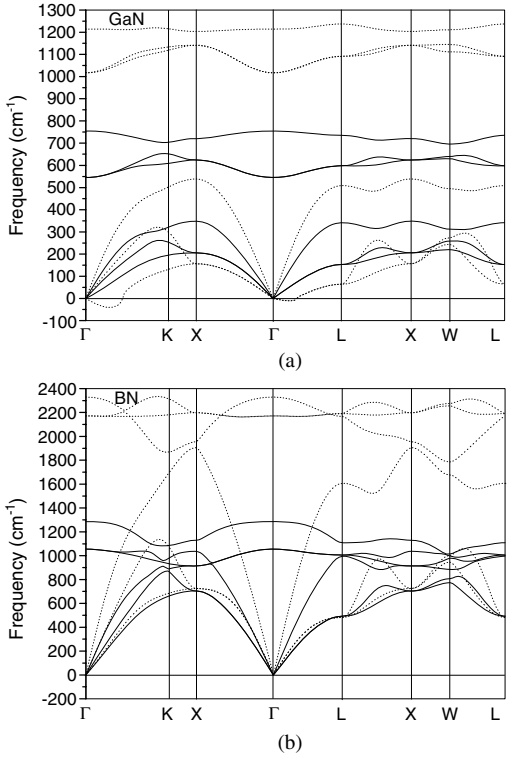

Figure 11. The first-principles phonon bands. (a) GaN phase, (b) BN phase. The solid curves are the phonon bands at $P = 0$ Mbar; the dotted curves are the phonon bands at $P = 2.19$ Mbar ($a/a_0 = 0.86$) and $P = 8.06$ Mbar ($a/a_0 = 0.80$) for GaN and BN, respectively.

more elastic energy is stored in the system. The system remains stable under force balance at a state of quite high internal energy. However, even a slight imbalance will cause rapid energy release and configuration change. A small shear strain at critical points destroys the force balance in the ZB phase and leads to phase transformation. From the above analysis, we see that the pressure sustained by a perfect ZB phase can be rather high. However, local shear strain can be established when lattice defects are present in the crystal. This kind of shear strain is the origin of phase transformation in the ZB phase when its shear elastic coefficients become small enough under pressure. Due to the wide variations in defect type and distribution in solids, it is expected that the defect-induced phase transformation will not occur at a fixed point but over a range of pressures. This probabilistic behaviour of phase transformation for solids under high pressure has been verified by extensive experimental observations, for example in high-pressure phase transformation experiments on ZnS [49–51], SiC [52, 53], InAs [54, 55], GaAs [56, 57] etc. It is important to mention the influence of thermodynamic vibration at finite temperature. Thermodynamic vibration enhances the force imbalance in solids and causes the critical point of phase transformation to shift to a lower state of hydrostatic pressure [9].

There are three fundamental questions for the matter of pressure-induced phase transformation. These are listed as when the phase transformation begins, how the structure changes during the transition and what the new structure is. These questions are among the main concerns in the theoretical study of phase transition in solids nowadays. We specifically investigate the condition of elastic stability of ZB III–V phases under pressure in the present

paper. The pressure-induced phase transition will be initiated as the structure loses elastic stability in these semiconductors. Besides, several pioneering first-principles works have also been done for the other two questions recently [58–61]. A comprehensive understanding of pressure-induced phase transformation can be achieved upon the answers of these questions.

5. Conclusions

The stress–strain relationships and elastic stabilities of GaP, InP, BN and GaN under hydrostatic pressure are investigated by first-principles calculations. Both work–energy and elastic-stiffness criteria are used in the lattice stability analysis. The two methods give completely the same result. Our study shows that the disappearance of the bulk modulus is the main reason for the loss of lattice stability of a perfect ZB phase under volume dilatation. The diminishing to zero of some elastic coefficients is considered as the main reason for phonon softening and elastic instability under pressure. It is pointed out that the experimentally observed high-pressure phase transformation is mainly due to lattice defects in the samples. The internal shear strains arise from these lattice defects and cause structural instability when the shear elastic-stiffness coefficients of the phase under high pressure become small. It is estimated that a perfect ZB phase should sustain much higher pressure than what has been experimentally reported thus far.

Acknowledgments

We are particularly grateful to Professor J Li and Dr X Lin for their help in using the Beowulf PC clusters in the Department of Nuclear Engineering at Massachusetts Institute of Technology and the Department of Materials Science and Engineering at Ohio State University. One of the authors (SQW) would like to thank the China Scholarship Council for its support by a CSC scholarship program (No 20491009). This work was partially supported by the Special Funds for the Major State Basic Research Projects of China (No G2000067104) and the National Natural Science Foundation of China (No 50472085).

References

[1] Born M and Huang K 1956 *Dynamical Theory of Crystal Lattices* (Oxford: Clarendon)
[2] Hill R 1975 *Math. Proc. Camb. Phil. Soc.* **77** 225
[3] Wang J, Yip S, Phillpot S R and Wolf D 1993 *Phys. Rev. Lett.* **71** 4182
[4] Morris J W and Krenn C R 2000 *Phil. Mag.* A **80** 2827
[5] Hill R and Milstein F 1977 *Phys. Rev.* B **15** 3087
[6] Wang J, Li J, Yip S, Phillpot S and Wolf D 1995 *Phys. Rev.* B **52** 12627
[7] Yip S, Li J, Tang M J and Wang J H 2001 *Mater. Sci. Eng.* A **317** 236
[8] Mizushima K, Tang M J and Yip S 1998 *J. Alloys Compounds* **279** 70
[9] Mizushima K, Yip S and Kaxiras E 1994 *Phys. Rev.* B **50** 14952
[10] Tang M and Yip S 1995 *Phys. Rev. Lett.* **75** 2738
[11] Tang M and Yip S 1995 *J. Appl. Phys.* **76** 2719
[12] Cleri F, Wang J and Yip S 1995 *J. Appl. Phys.* **77** 1449
[13] Kocer C, Hirosaki N and Ogata S 2003 *Phys. Rev.* B **67** 35210
[14] Sob M, Wang L G and Vitek V 1997 *Mater. Sci. Eng.* A **234** 1075
[15] Roundy D, Krenn C R, Cohen M L and Morris J W 1999 *Phys. Rev. Lett.* **82** 2713
[16] Roundy D, Krenn C R, Cohen M L and Morris J W 2001 *Phil. Mag.* A **81** 1725
[17] Ogata S, Hirosaki N, Kocer C and Kitagawa H 2001 *Phys. Rev.* B **64** 172102
[18] Luo W, Roundy D, Cohen M L and Morris J W 2002 *Phys. Rev.* B **66** 94110
[19] Clatterbuck D M, Chrzan D C and Morris J W 2002 *Phil. Mag. Lett.* **82** 141

[20] Clatterbuck D M, Chrzan D C and Morris J W 2003 *Acta Mater.* **51** 2271
[21] Wang S Q and Ye H Q 2002 *J. Phys.: Condens. Matter* **14** 9579
[22] Wang S Q and Ye H Q 2005 *J. Phys.: Condens. Matter* **17** 4475
[23] Wang S Q and Ye H Q 2003 *J. Phys.: Condens. Matter* **15** 5307
[24] Wang S Q and Ye H Q 2003 *Phys. Status Solidi* b **240** 45
[25] Wang S Q and Ye H Q 2003 *J. Phys.: Condens. Matter* **15** L197
[26] Phillips J C 1973 *Bonds and Bands in Semiconductors* (New York: Academic)
[27] Mooser E and Pearson W B 1959 *Acta Crystallogr.* A **12** 1015
[28] Parthe E 1964 *Crystal Chemistry of Tetrahedral Structures* (New York: Gordon and Breach)
[29] Gonze X, Beuken J M, Caracas R, Detraux F, Fuchs M, Rignanese G M, Sindic L, Verstraete M, Zerah G, Jollet F, Torrent M, Roy A, Mikami M, Ghosez P, Raty J Y and Allan D C 2002 *Comput. Mater. Sci.* **25** 478
[30] Hartwigsen C, Goedecker S and Hutter J 1998 *Phys. Rev.* B **58** 3641
[31] Steinle-Neumann G, Stixrude L and Cohen R E 1999 *Phys. Rev.* B **60** 791
[32] Nielsen O H and Martin R M 1985 *Phys. Rev.* B **32** 3780
[33] Nielsen O H and Martin R M 1985 *Phys. Rev.* B **32** 3792
[34] Wallace D C 1972 *Thermodynamics of Crystal* (New York: Wiley)
[35] Polian A and Grimsditch M 1999 *Phys. Rev.* B **60** 1468
[36] Birch F 1947 *Phys. Rev.* **71** 809
[37] Vinet P, Ferrante J, Smith J R and Rose J H 1986 *J. Phys. C: Solid State Phys.* **19** L467
[38] Kleinman L 1962 *Phys. Rev.* **128** 2614
[39] Kim K, Lambrecht W R L and Segall B 1996 *Phys. Rev.* B **53** 16310
[40] de Gironcoli S, Baroni S and Resta R 1989 *Phys. Rev. Lett.* **62** 2853
[41] Christensen N E, Satpathy S and Pawlowska Z 1987 *Phys. Rev.* B **36** 1032
[42] Rodriguez-Hernandez P, Gonzalez-Diaz M and Munoz A 1995 *Phys. Rev.* B **51** 14705
[43] Cousins C S G 1978 *J. Phys. C: Solid State Phys.* **11** 4867
[44] Cousins C S G 1978 *J. Phys. C: Solid State Phys.* **11** 4881
[45] Cousins C S G 1982 *J. Phys. C: Solid State Phys.* **15** 1857
[46] Cousins C S G 2003 *Phys. Rev.* B **67** 24107
[47] Baroni S, de Gironcoli S, Corso A D and Giannozzi P 2001 *Rev. Mod. Phys.* **73** 515
[48] Prikhodko M, Miao M S and Lambrecht W R L 2002 *Phys. Rev.* B **66** 125201
[49] Samara G A and Drickamer H G 1962 *J. Phys. Chem. Solids* **23** 457
[50] Desgreniers S, Beaulieu L and Lepage I 2000 *Phys. Rev.* B **61** 8726
[51] Ves S, Schwarz U, Christensen N E, Syassen K and Cardona M 1990 *Phys. Rev.* B **42** 9113
[52] Yoshida M, Onodera A, Ueno M, Takemura K and Shimomura O 1993 *Phys. Rev.* B **48** R10587
[53] Sekine T and Kobayashi T 1997 *Phys. Rev.* B **55** 8034
[54] Minomura S and Drickamer H G 1962 *J. Phys. Chem. Solids* **23** 451
[55] Pitt G D and Vyas M K R 1973 *J. Phys. C: Solid State Phys.* **6** 274
[56] Besson J M, Itie J P, Polian A, Weill G, Mansot J L and Gonzalez J 1991 *Phys. Rev.* B **44** 4214
[57] Weir S T, Vohra Y K, Vanderborgh C A and Ruoff A L 1989 *Phys. Rev.* B **39** 1280
[58] Catti M 2001 *Phys. Rev. Lett.* **87** 35504
[59] Miao M S and Lambrecht W R L 2003 *Phys. Rev.* B **68** 92103
[60] Catti M 2002 *Phys. Rev.* B **65** 224115
[61] Miao M S and Lambrecht W R L 2005 *Phys. Rev. Lett.* **94** 225501